Laminar optical tomography: demonstration of millimeter-scale depth-resolved imaging in turbid media

Elizabeth M. C. Hillman, David A. Boas, Anders M. Dale, and Andrew K. Dunn

Martinos Center for Biomedical Imaging, Massachusetts General Hospital, Harvard Medical School, Building 149, 13th Street, Charlestown, Massachusetts 02129

Received February 25, 2004

Laminar optical tomography (LOT) is a new technique that combines the advantages of diffuse optical tomography image reconstruction and a microscopy-based setup to allow noncontact imaging with 100−200-μm resolution effective over depths of 0−2.5 mm. LOT is being developed primarily for multispectral imaging of rat cortex, for which resolving functional dynamics in various layers of the brain's cortex (to depths of 1500 μm) is of increasing interest to neurophysiologists. System design and image reconstruction techniques are described, along with simulation and phantom results that demonstrate the characteristics and limitations of system accuracy and resolution.

OCIS codes: 170.0170, 170.6900, 170.6960, 170.3890, 170.3880.

Diffuse optical tomography (DOT) is conventionally used to image the brain through intact skull.[1] Topographic arrangements of sources and detectors can yield images of functional activity at depths of a few centimeters, with centimeter resolution. Confocal microscopy can yield micrometer resolution images of living tissue but has the ability to image only superficially. Bridging the gap between micrometer and centimeter depth sensitivity and resolution, laminar optical tomography (LOT) combines DOT techniques for image reconstruction with a microscopy-based setup to allow imaging with ~200-μm resolution over depths of 0−2.5 mm. LOT therefore surpasses the depth capabilities of optical coherence tomography and, although it has lower spatial resolution, is better suited to spectroscopy, as multiple narrowband sources can be used.

The primary target for this imaging system is the cortex of the rat. Researchers are increasingly using rodent models to investigate cortical hemodynamics and neurophysiology. The role of the different layers of the cortex has only recently been preliminarily examined by use of high-resolution functional MRI[2] and optical coherence tomography.[3] Thinned-skull preparations provide an area of approximately 4 mm × 4 mm, where regions of activation that correspond to stimuli such as passive whisker or forepaw movements can be localized in two dimensions by use of optical techniques such as multispectral, laser Doppler, and speckle-flow imaging. Recent results that revealed the time courses of activation, neurovascular coupling, and spreading depression with such techniques have already demonstrated the huge potential effect of such studies on neuroimaging.[4–7] LOT has the ability to extend these observations to three dimensions, to allow dynamic characteristics to be attributed to specific cortical layers. In addition, LOT data can feasibly be acquired simultaneously with other measurements such as speckle-flow imaging, and the LOT system can readily be modified to measure fluorescence contrast in addition to absorption changes.

LOT instrumentation acquires measurements that are equivalent to conventional DOT data, specifically, the scattered light emerging from tissue, for a variety of source and detector positions over the area of interest. It is not desirable to use contact-based fibers for delivery and collection of light in a rat cortical imaging experiment. Instead, LOT uses a system based on a confocal microscope design, coupling laser light into and out of the target via lenses and changing the location of the illumination by use of a pair of galvanometer mirrors (Cambridge Technologies). There are several ways to measure the light emerging from tissue at a series of distances from the point of illumination, for example, by processing a CCD image of the moving spot, or a similar measure can be derived by use of patterned illumination as described in Ref. 8. Our LOT system utilizes seven avalanche photodiode detectors (Hamamatsu KK). Each avalanche photodiode is connected to a 200-μm fiber, whose other end is part of a linear fiber bundle positioned in the system as shown in Fig. 1. The moving galvanometer mirrors image the light that comes from the illuminated spot back along the same optical axis as the delivered light. In LOT, one of the seven fibers in the fiber bundle is aligned with the optical axis, collecting confocal data, but the other six fibers collect light coming from six successive equally spaced distances away from the illuminated spot. As the laser beam scans, each avalanche photodiode compiles an image that corresponds to the light emerging at one of the six fixed distances away from the beam's focus. In the current configuration, the illuminated spot scans an adjustable field of view of approximately 3 mm × 3 mm, and the farthest detection fiber maps to 1.5 mm away from the illuminating spot. Currently, a set of seven 25 × 25 pixel images can be acquired simultaneously in ~0.4 s with 1-mW illumination from a 532-nm Nd:YVO_4 laser, although this rate is limited primarily by the current PC card acquisition rate (10 kHz/channel) and ultimately by galvanometer step response times.

Raw data acquired with the LOT system reveal features of the different layers that correspond to the different source−detector separations. Figure 2 compares a CCD image with LOT raw images of

0146-9592/04/141650-03$15.00/0

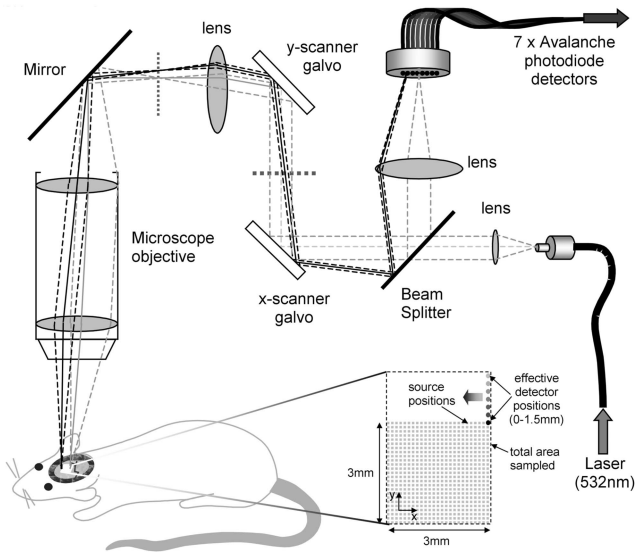

Fig. 1. LOT system design. Galvanometer mirrors steer a focused spot over an adjustable (e.g., 3 mm × 3 mm) area. Multiple detectors acquire data from successive distances away from the focused spot. The total area sampled is typically 3 mm × 4.5 mm, representing the area raster-scanned by the source, and the imaged y-displaced detectors.

the same field of view. Where the CCD image uses diffuse illumination, revealing the vessels on the surface of the brain with high contrast because light is backscattered from the underlying brain, the LOT images isolate features of various layers, depending on the separation of the source and the detector (the 0-mm LOT image shows features of the surface of the thinned skull, whereas the 1.13-mm image isolates deeper vessels). Such results were used previously to reveal age-related macular degeneration in the retina by use of off-axis illumination in a commercial ophthalmic confocal imaging instrument (although with smaller effective source detector spacings from those in LOT).[9] Multiple transmitter–receiver separations have also been used for (nonimaging) laser-Doppler measurements to resolve depth-dependent cortical blood flow characteristics.[10] However, although they are qualitatively useful, surface features as well as the slight lateral displacement of each raw LOT depth image can complicate interpretation of the true depth of the observed features. Therefore it is desirable to attempt to reconstruct the three-dimensional properties of the tissue that is being imaged from the measured data set.

Image reconstruction in DOT generally utilizes the diffusion approximation. However, the diffusion approximation is not a suitable model for LOT, as the source–detector separations are of the order of the tissue's scattering length. Therefore, Monte Carlo modeling is used instead to generate source and detector flux distributions, which are then used to derive Born-approximation-based weight functions $J_{s,d}(r)$ that represent the sensitivity of each measurement (s, d) to changes in $\mu_a(r)$. Correct generation of $J_{s,d}(r)$ is described in detail in Ref. 11, but the most important consideration is to account correctly for the directional components of the photon flux rather than to use the integrated photon fluence as is usual for DOT. Once $J_{s,d}(r)$is generated, image reconstruction can then be achieved by means of Tikhonov regularization:

$$\Delta\boldsymbol{\mu}_a = \mathbf{J}^{\mathbf{T}}(\mathbf{J}\mathbf{J}^{\mathbf{T}} + \lambda I)^{-1}\,\frac{\Delta\mathbf{M}\mathbf{L}_0}{\mathbf{M}_0}\,, \tag{1}$$

where $\Delta\mathbf{M}$ are changes in measurement between an unperturbed state ($\mathbf{M}_0$) and a perturbed state, $\mathbf{J}$ is the set of $J_{s,d}(r)$, $\Delta\mu_a$ is the image of $\mu_a(r)$ changes sought, and $\mathbf{L}_0$ are Monte Carlo–simulated unperturbed measurements. $\lambda = \alpha \times \max[\mathrm{diag}(\mathbf{J}\mathbf{J}^T)]$, where regularization parameter α effectively controls the influence of model mismatch, noise, and systematic errors on the reconstructed image (at the expense of image resolution, accuracy, and quantitation). Normalizing by $\mathbf{M}_0$ reduces the effect of systematic spatial variations in throughput, and using differential measurement $\Delta\mathbf{M}$ reduces the effects of system reflections. $\mathbf{M}_0$ is reflection-corrected by subtraction of a measurement made by placing a beam dump in the object plane.

Figure 3 shows LOT images of a phantom consisting of a human hair (~100-μm diameter), positioned at different depths in a dish of Intralipid and bovine hemoglobin ($\mu_a \sim 0.1\ \mathrm{mm}^{-1}$, $\mu_s' \sim 1\ \mathrm{mm}^{-1}$ at 532 nm). Unperturbed-state data were acquired with only the Intralipid solution and no hair. The hair was then carefully lowered into the Intralipid by a micrometer stage, with 100 × 100 × 7 LOT measurements acquired for each selected hair depth. The measurement geometry is illustrated in Fig. 1; the hair was diagonally positioned in the x–y plane (and horizontally in the z plane). The source and detector positions were raster scanned, covering a total sample area of 3 mm × 4.5 mm, with the detectors effectively displaced up to 1.5 mm away from the source along the y direction. Acquired data were downsampled to a 12 × 12 grid, and reconstructions were performed within a 14 × 20 × 20 voxel region by use of Eq. (1) (each voxel was 230 μm × 230 μm × 100 μm). The weight functions were generated by means of a Monte Carlo simulation with 10^7 photons, $\mu_a = 0.1\ \mathrm{mm}^{-1}$, $\mu_s = 10\ \mathrm{mm}^{-1}$, and $g = 0.9$. The regularization parameter α was chosen to yield an image maximum of $\Delta\mu_a = 0.1\ \mathrm{mm}^{-1}$ for each data set (0.9, 0.025, 0.0015, and 0.0004 for 0, 400, 800, and

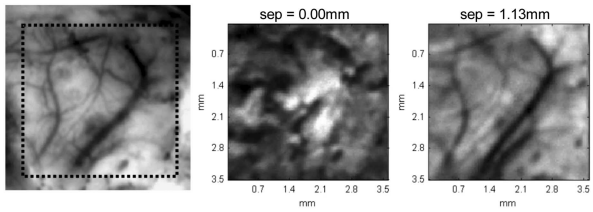

Fig. 2. Center and right, high resolution (100 × 100) raw images from the LOT system for two source–detector separations on rat cortex through thinned-skull at 532 nm. The 0-mm image shows the reflectance of the skull surface, whereas the 1.13-mm image isolates features of the cortical vasculature. Left, simultaneously acquired CCD image of the same region with diffuse 580-nm illumination.

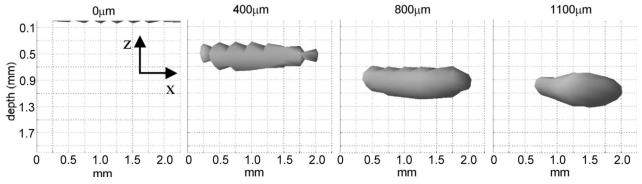

Fig. 3. Reconstructed images of a human hair (~100-μm diameter) positioned at 0-, 400-, 800-, and 1100-μm depths ($\pm$50 μm) in Intralipid and bovine hemoglobin. $\Delta\mu_a$ = 0.075 mm^{-1} isosurfaces shown in an $x-z$ view.

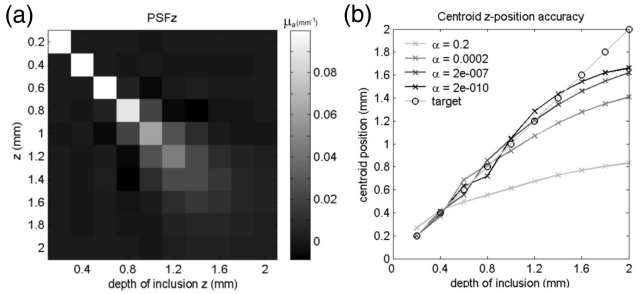

Fig. 4. Left, z-direction point-spread functions for a 0.1-mm^{-1} $\Delta\mu_a$ perturbation at various depths ($\alpha = 10^{-10}$). Right, z-centroid positions of each perturbation as a function of its depth for various values of α.

1100 μm, respectively). Figure 3 shows isosurfaces of a 2 mm $\times$ 2.1 mm $\times$ 2.1 mm subregion of the three-dimensional solution, in the $x-z$ plane, each representing 75% maximum of the image (35% for the 0-mm image). Where z resolution clearly degrades with depth, the z location of the hair is clearly identified in each case. Other projections of the solution reveal that x–y resolution is maintained well with depth and is generally limited by the number of voxels used in the reconstruction.

Figure 4 presents simulations based on the phantom acquisition geometry to explore the limits of image quality achievable for this LOT configuration. Rather than generating forward data by use of the full Monte Carlo code and then separately reconstructing many images, one can derive the point-spread function for our system directly:

$$\Delta\boldsymbol{\mu}_a = \mathbf{J}^T(\mathbf{J}\mathbf{J}^T + \lambda I)^{-1}\mathbf{J}\Delta\tilde{\boldsymbol{\mu}}_a\,, \qquad (2)$$

where $\Delta\tilde{\mu}_a$ is the target change in absorption and $\Delta\mu_a$ is the absorption change that would be the result of a reconstruction. Figure 4(a) shows z-direction point spread functions (PSFs) for an object at various depths ($\alpha = 10^{-10}$). Figure 4(b) shows plots of the centroid position accuracy with depth for a variety of regularization parameters (α), demonstrating the potential improvements in performance that are achievable if the signal-to-noise ratio, calibration, and model accuracy are further optimized. For these simulations the background medium was assumed to have $\mu_a = 0.1$ mm^{-1}, $\mu_s = 10$ mm^{-1}, and $g = 0.9$, with a maximum effective separation between source and detector of 1.5 mm. Further simulations have revealed that increasing the effective separation between source and detectors improves amplitude accuracy with depth, but still results in fairly significant degradation for deeper perturbations (and the signal-to-noise ratio degrades for wider separation in practice). Considering a medium with a scattering coefficient of only 0.5 mm^{-1} also yields results with improved depth accuracy and localization, but again not without significant decay in quality with depth. These results imply that LOT can achieve higher resolution and accuracy than is typically associated with DOT techniques over the 0–1.2-mm depth range and that resolution and accuracy are likely to be more typical of diffuse imaging for deeper perturbations.

In summary, both theoretical and experimental validations of the LOT technique have been shown to demonstrate its potential for imaging tissue over length scales of a few millimeters. Improving the system's configuration and signal-to-noise ratio, as well as implementing more-advanced reconstruction techniques such as depth- and noise-dependent regularization, should continue to improve the performance of LOT. Fluorescence LOT will allow molecular probes and voltage sensitive dyes to be imaged alongside cortical hemodynamic parameters. Additional applications of LOT may also exist outside the neuroscience field, for example, in dermal, ocular, or cervical imaging.

The authors acknowledge support from National Institutes of Health grants (NS41291-01 and EB000790-01A2) and from the Whitaker Foundation. E. M. C. Hillman's e-mail address is ehillman@nmr.mgh.harvard.edu.

References

1. M. A. Franceschini, V. Toronov, M. E. Filiaci, E. Gratton, and S. Fantini, Opt. Express **6,** 49 (2000), http://www.opticsexpress.org.
2. A. C. Silva and A. P. Koretsky, Proc. Natl. Acad. Sci. USA **99,** 15,182 (2002).
3. R. Uma Maheswari, H. Takaoka, H. Kadono, R. Honma, and M. Tanifuji, J. Neurosci. Meth. **124,** 83 (2003).
4. A. M. Ba, M. Guiou, N. Pouratian, A. Muthialu, D. E. Rex, A. F. Cannestra, J. W. Y. Chen, and A. W. Toga, J. Neurophysiol. **88,** 2726 (2002).
5. H. Bolay, U. Reuter, A. Dunn, D. Boas, and M. Moskowitz, Nature Med. **8,** 136 (2002).
6. M. Jones, J. Berwick, D. Johnston, and J. Mayhew, Neuroimage **13,** 1002 (2001).
7. C. C. Petersen, A. Grinvald, and B. Sakmann, J. Neurosci. **23,** 1298 (2003).
8. F. Bevilacqua, D. J. Cuccia, A. J. Durkin, and B. J. Tromberg, in *Biomedical Topical Meetings*, Vol. 71 of OSA Trends in Optics and Photonics Series (Optical Society of America, Washington, D.C., 2002), pp. 677–679.
9. A. E. Elsner, Q. Zhou, F. Beck, P. E. Tornambe, S. A. Burns, J. J. Weiter, and A. W. Dreher, Int. Ophthalmol. **23,** 245 (2001).
10. M. Fabricius, N. Akgören, U. Dirnagl, and M. Lauritzen, J. Cereb. Blood Flow Metab. **17,** 1326 (1997).
11. A. Dunn and D. Boas, Opt. Lett. **25,** 1777 (2000).